DELPHI Collaboration

DELPHI 2004-034-CONF-709
10 June, 2004

Flavour-Independent Searches for Neutral Higgs Bosons decaying into hadrons with the DELPHI Detector at LEP2

P. Bambade
LAL, Orsay
M. Boonekamp
CEA, Saclay
G. Borisov
University of Lancaster
M. Stanitzki
Inst. für Exper. Kernphysik, Karlsruhe
E. Graziani
Roma III / INFN
I. van Vulpen
CERN

Abstract

Flavour-independent searches for neutral Higgs bosons decaying hadronically are described, using data collected by the DELPHI experiment at LEP in e^+e^- collisions at centre-of-mass energies between 189 and 209 GeV. The collected data-set corresponds to an integrated luminosity of around 610 pb^{-1}. Both hZ and hA productions with direct decays into hadrons have been considered. These searches are more general than the usual Standard Model (SM) or Minimal Supersymmetric Standard Model (MSSM) Higgs boson searches, and lead to results interpretable in a wide range of models. No evidence for Higgs boson production was found and limits on hZ and hA production cross-sections were set as a function of the Higgs boson masses.

Contributed Paper for ICHEP 2004 (Beijing)

EUROPEAN ORGANIZATION FOR NUCLEAR RESEARCH

CERN–EP-Paper 330 - Draft 2.

5 January 2004

Flavour-Independent Searches for Neutral Higgs Bosons decaying into hadrons with the DELPHI Detector at LEP2

DELPHI Collaboration

Abstract

Flavour-independent searches for neutral Higgs bosons decaying hadronically are described, using data collected by the DELPHI experiment at LEP in e^+e^- collisions at centre-of-mass energies between 189 and 209 GeV. The collected data-set corresponds to an integrated luminosity of around 610 pb^{-1}. Both hZ and hA productions with direct decays into hadrons have been considered. These searches are more general than the usual Standard Model (SM) or Minimal Supersymmetric Standard Model (MSSM) Higgs boson searches, and lead to results interpretable in a wide range of models. No evidence for Higgs boson production was found and limits on hZ and hA production cross-sections were set as a function of the Higgs boson masses.

Send comments up to 14/01/2004 to
Ivo.Vanvulpen@cern.ch,
g.myatt1@physics.ox.ac.uk(Editor),
Achille.Stocchi@cern.ch, Dimartino@axdeof.cern.ch
Reader's Board : Wolfgang.Adam@cern.ch,Ruhlmann@in2p3.fr

J.Abdallah[25], P.Abreu[22], W.Adam[51], P.Adzic[11], T.Albrecht[17], T.Alderweireld[2], R.Alemany-Fernandez[8], T.Allmendinger[17], P.P.Allport[23], U.Amaldi[29], N.Amapane[45], S.Amato[48], E.Anashkin[36], A.Andreazza[28], S.Andringa[22], N.Anjos[22], P.Antilogus[25], W-D.Apel[17], Y.Arnoud[14], S.Ask[26], B.Asman[44], J.E.Augustin[25], A.Augustinus[8], P.Baillon[8], A.Ballestrero[46], P.Bambade[20], R.Barbier[27], D.Bardin[16], G.Barker[17], A.Baroncelli[39], M.Battaglia[8], M.Baubillier[25], K-H.Becks[53], M.Begalli[6], A.Behrmann[53], E.Ben-Haim[20], N.Benekos[32], A.Benvenuti[5], C.Berat[14], M.Berggren[25], L.Berntzon[44], D.Bertrand[2], M.Besancon[40], N.Besson[40], D.Bloch[9], M.Blom[31], M.Bluj[52], M.Bonesini[29], M.Boonekamp[40], P.S.L.Booth[23], G.Borisov[21], O.Botner[49], B.Bouquet[20], T.J.V.Bowcock[23], I.Boyko[16], M.Bracko[43], R.Brenner[49], E.Brodet[35], P.Bruckman[18], J.M.Brunet[7], L.Bugge[33], P.Buschmann[53], M.Calvi[29], T.Camporesi[8], V.Canale[38], F.Carena[8], N.Castro[22], F.Cavallo[5], M.Chapkin[42], Ph.Charpentier[8], P.Checchia[36], R.Chierici[8], P.Chliapnikov[42], J.Chudoba[8], S.U.Chung[8], K.Cieslik[18], P.Collins[8], R.Contri[13], G.Cosme[20], F.Cossutti[47], M.J.Costa[50], D.Crennell[37], J.Cuevas[34], J.D'Hondt[2], J.Dalmau[44], T.da Silva[48], W.Da Silva[25], G.Della Ricca[47], A.De Angelis[47], W.De Boer[17], C.De Clercq[2], B.De Lotto[47], N.De Maria[45], A.De Min[36], L.de Paula[48], L.Di Ciaccio[38], A.Di Simone[39], K.Doroba[52], J.Drees[53,8], M.Dris[32], G.Eigen[4], T.Ekelof[49], M.Ellert[49], M.Elsing[8], M.C.Espirito Santo[22], G.Fanourakis[11], D.Fassouliotis[11,3], M.Feindt[17], J.Fernandez[41], A.Ferrer[50], F.Ferro[13], U.Flagmeyer[53], H.Foeth[8], E.Fokitis[32], F.Fulda-Quenzer[20], J.Fuster[50], M.Gandelman[48], C.Garcia[50], Ph.Gavillet[8], E.Gazis[32], R.Gokieli[8,52], B.Golob[43], G.Gomez-Ceballos[41], P.Goncalves[22], E.Graziani[39], G.Grosdidier[20], K.Grzelak[52], J.Guy[37], C.Haag[17], A.Hallgren[49], K.Hamacher[53], K.Hamilton[35], S.Haug[33], F.Hauler[17], V.Hedberg[26], M.Hennecke[17], H.Herr[8], J.Hoffman[52], S-O.Holmgren[44], P.J.Holt[8], M.A.Houlden[23], K.Hultqvist[44], J.N.Jackson[23], G.Jarlskog[26], P.Jarry[40], D.Jeans[35], E.K.Johansson[44], P.D.Johansson[44], P.Jonsson[27], C.Joram[8], L.Jungermann[17], F.Kapusta[25], S.Katsanevas[27], E.Katsoufis[32], G.Kernel[43], B.P.Kersevan[8,43], U.Kerzel[17], A.Kiiskinen[15], B.T.King[23], N.J.Kjaer[8], P.Kluit[31], P.Kokkinias[11], C.Kourkoumelis[3], O.Kouznetsov[16], Z.Krumstein[16], M.Kucharczyk[18], J.Lamsa[1], G.Leder[51], F.Ledroit[14], L.Leinonen[44], R.Leitner[30], J.Lemonne[2], V.Lepeltier[20], T.Lesiak[18], W.Liebig[53], D.Liko[51], A.Lipniacka[44], J.H.Lopes[48], J.M.Lopez[34], D.Loukas[11], P.Lutz[40], L.Lyons[35], J.MacNaughton[51], A.Malek[53], S.Maltezos[32], F.Mandl[51], J.Marco[41], R.Marco[41], B.Marechal[48], M.Margoni[36], J-C.Marin[8], C.Mariotti[8], A.Markou[11], C.Martinez-Rivero[41], J.Masik[12], N.Mastroyiannopoulos[11], F.Matorras[41], C.Matteuzzi[29], F.Mazzucato[36], M.Mazzucato[36], R.Mc Nulty[23], C.Meroni[28], E.Migliore[45], W.Mitaroff[51], U.Mjoernmark[26], T.Moa[44], M.Moch[17], K.Moenig[8,10], R.Monge[13], J.Montenegro[31], D.Moraes[48], S.Moreno[22], P.Morettini[13], U.Mueller[53], K.Muenich[53], M.Mulders[31], L.Mundim[6], W.Murray[37], B.Muryn[19], G.Myatt[35], T.Myklebust[33], M.Nassiakou[11], F.Navarria[5], K.Nawrocki[52], R.Nicolaidou[40], M.Nikolenko[16,9], A.Oblakowska-Mucha[19], V.Obraztsov[42], A.Olshevski[16], A.Onofre[22], R.Orava[15], K.Osterberg[15], A.Ouraou[40], A.Oyanguren[50], M.Paganoni[29], S.Paiano[5], J.P.Palacios[23], H.Palka[18], Th.D.Papadopoulou[32], L.Pape[8], C.Parkes[24], F.Parodi[13], U.Parzefall[8], A.Passeri[39], O.Passon[53], L.Peralta[22], V.Perepelitsa[50], A.Perrotta[5], A.Petrolini[13], J.Piedra[41], L.Pieri[39], F.Pierre[40], M.Pimenta[22], E.Piotto[8], T.Podobnik[43], V.Poireau[8], M.E.Pol[6], G.Polok[18], P.Poropat[47], V.Pozdniakov[16], N.Pukhaeva[2,16], A.Pullia[29], J.Rames[12], L.Ramler[17], A.Read[33], P.Rebecchi[8], J.Rehn[17], D.Reid[31], R.Reinhardt[53], P.Renton[35], F.Richard[20], J.Ridky[12], M.Rivero[41], D.Rodriguez[41], A.Romero[45], P.Ronchese[36], P.Roudeau[20], T.Rovelli[5], V.Ruhlmann-Kleider[40], D.Ryabtchikov[42], A.Sadovsky[16], L.Salmi[15], J.Salt[50], A.Savoy-Navarro[25], U.Schwickerath[8], A.Segar[35], R.Sekulin[37], M.Siebel[53], A.Sisakian[16], G.Smadja[27], O.Smirnova[26], A.Sokolov[42], A.Sopczak[21], R.Sosnowski[52], T.Spassov[8], M.Stanitzki[17], A.Stocchi[20], J.Strauss[51], B.Stugu[4], M.Szczekowski[52], M.Szeptycka[52], T.Szumlak[19], T.Tabarelli[29], A.C.Taffard[23], F.Tegenfeldt[49], J.Timmermans[31], L.Tkatchev[16], M.Tobin[23], S.Todorovova[12], B.Tome[22], A.Tonazzo[29], P.Tortosa[50], P.Travnicek[12], D.Treille[8], G.Tristram[7], M.Trochimczuk[52], C.Troncon[28], M-L.Turluer[40], I.A.Tyapkin[16], P.Tyapkin[16], S.Tzamarias[11], V.Uvarov[42], G.Valenti[5], P.Van Dam[31], J.Van Eldik[8], A.Van Lysebetten[2], N.van Remortel[2], I.Van Vulpen[8], G.Vegni[28], F.Veloso[22], W.Venus[37], P.Verdier[27], V.Verzi[38], D.Vilanova[40], L.Vitale[47], V.Vrba[12],

H.Wahlen[53], A.J.Washbrook[23], C.Weiser[17], D.Wicke[8], J.Wickens[2], G.Wilkinson[35], M.Winter[9], M.Witek[18], O.Yushchenko[42], A.Zalewska[18], P.Zalewski[52], D.Zavrtanik[43], V.Zhuravlov[16], N.I.Zimin[16], A.Zintchenko[16], M.Zupan[11]

[1]Department of Physics and Astronomy, Iowa State University, Ames IA 50011-3160, USA
[2]Physics Department, Universiteit Antwerpen, Universiteitsplein 1, B-2610 Antwerpen, Belgium
and IIHE, ULB-VUB, Pleinlaan 2, B-1050 Brussels, Belgium
and Faculté des Sciences, Univ. de l'Etat Mons, Av. Maistriau 19, B-7000 Mons, Belgium
[3]Physics Laboratory, University of Athens, Solonos Str. 104, GR-10680 Athens, Greece
[4]Department of Physics, University of Bergen, Allégaten 55, NO-5007 Bergen, Norway
[5]Dipartimento di Fisica, Università di Bologna and INFN, Via Irnerio 46, IT-40126 Bologna, Italy
[6]Centro Brasileiro de Pesquisas Físicas, rua Xavier Sigaud 150, BR-22290 Rio de Janeiro, Brazil
and Depto. de Física, Pont. Univ. Católica, C.P. 38071 BR-22453 Rio de Janeiro, Brazil
and Inst. de Física, Univ. Estadual do Rio de Janeiro, rua São Francisco Xavier 524, Rio de Janeiro, Brazil
[7]Collège de France, Lab. de Physique Corpusculaire, IN2P3-CNRS, FR-75231 Paris Cedex 05, France
[8]CERN, CH-1211 Geneva 23, Switzerland
[9]Institut de Recherches Subatomiques, IN2P3 - CNRS/ULP - BP20, FR-67037 Strasbourg Cedex, France
[10]Now at DESY-Zeuthen, Platanenallee 6, D-15735 Zeuthen, Germany
[11]Institute of Nuclear Physics, N.C.S.R. Demokritos, P.O. Box 60228, GR-15310 Athens, Greece
[12]FZU, Inst. of Phys. of the C.A.S. High Energy Physics Division, Na Slovance 2, CZ-180 40, Praha 8, Czech Republic
[13]Dipartimento di Fisica, Università di Genova and INFN, Via Dodecaneso 33, IT-16146 Genova, Italy
[14]Institut des Sciences Nucléaires, IN2P3-CNRS, Université de Grenoble 1, FR-38026 Grenoble Cedex, France
[15]Helsinki Institute of Physics, P.O. Box 64, FIN-00014 University of Helsinki, Finland
[16]Joint Institute for Nuclear Research, Dubna, Head Post Office, P.O. Box 79, RU-101 000 Moscow, Russian Federation
[17]Institut für Experimentelle Kernphysik, Universität Karlsruhe, Postfach 6980, DE-76128 Karlsruhe, Germany
[18]Institute of Nuclear Physics,Ul. Kawiory 26a, PL-30055 Krakow, Poland
[19]Faculty of Physics and Nuclear Techniques, University of Mining and Metallurgy, PL-30055 Krakow, Poland
[20]Université de Paris-Sud, Lab. de l'Accélérateur Linéaire, IN2P3-CNRS, Bât. 200, FR-91405 Orsay Cedex, France
[21]School of Physics and Chemistry, University of Lancaster, Lancaster LA1 4YB, UK
[22]LIP, IST, FCUL - Av. Elias Garcia, 14-1^{o}, PT-1000 Lisboa Codex, Portugal
[23]Department of Physics, University of Liverpool, P.O. Box 147, Liverpool L69 3BX, UK
[24]Dept. of Physics and Astronomy, Kelvin Building, University of Glasgow, Glasgow G12 8QQ
[25]LPNHE, IN2P3-CNRS, Univ. Paris VI et VII, Tour 33 (RdC), 4 place Jussieu, FR-75252 Paris Cedex 05, France
[26]Department of Physics, University of Lund, Sölvegatan 14, SE-223 63 Lund, Sweden
[27]Université Claude Bernard de Lyon, IPNL, IN2P3-CNRS, FR-69622 Villeurbanne Cedex, France
[28]Dipartimento di Fisica, Università di Milano and INFN-MILANO, Via Celoria 16, IT-20133 Milan, Italy
[29]Dipartimento di Fisica, Univ. di Milano-Bicocca and INFN-MILANO, Piazza della Scienza 2, IT-20126 Milan, Italy
[30]IPNP of MFF, Charles Univ., Areal MFF, V Holesovickach 2, CZ-180 00, Praha 8, Czech Republic
[31]NIKHEF, Postbus 41882, NL-1009 DB Amsterdam, The Netherlands
[32]National Technical University, Physics Department, Zografou Campus, GR-15773 Athens, Greece
[33]Physics Department, University of Oslo, Blindern, NO-0316 Oslo, Norway
[34]Dpto. Fisica, Univ. Oviedo, Avda. Calvo Sotelo s/n, ES-33007 Oviedo, Spain
[35]Department of Physics, University of Oxford, Keble Road, Oxford OX1 3RH, UK
[36]Dipartimento di Fisica, Università di Padova and INFN, Via Marzolo 8, IT-35131 Padua, Italy
[37]Rutherford Appleton Laboratory, Chilton, Didcot OX11 OQX, UK
[38]Dipartimento di Fisica, Università di Roma II and INFN, Tor Vergata, IT-00173 Rome, Italy
[39]Dipartimento di Fisica, Università di Roma III and INFN, Via della Vasca Navale 84, IT-00146 Rome, Italy
[40]DAPNIA/Service de Physique des Particules, CEA-Saclay, FR-91191 Gif-sur-Yvette Cedex, France
[41]Instituto de Fisica de Cantabria (CSIC-UC), Avda. los Castros s/n, ES-39006 Santander, Spain
[42]Inst. for High Energy Physics, Serpukov P.O. Box 35, Protvino, (Moscow Region), Russian Federation
[43]J. Stefan Institute, Jamova 39, SI-1000 Ljubljana, Slovenia and Laboratory for Astroparticle Physics,
Nova Gorica Polytechnic, Kostanjeviska 16a, SI-5000 Nova Gorica, Slovenia,
and Department of Physics, University of Ljubljana, SI-1000 Ljubljana, Slovenia
[44]Fysikum, Stockholm University, Box 6730, SE-113 85 Stockholm, Sweden
[45]Dipartimento di Fisica Sperimentale, Università di Torino and INFN, Via P. Giuria 1, IT-10125 Turin, Italy
[46]INFN,Sezione di Torino, and Dipartimento di Fisica Teorica, Università di Torino, Via P. Giuria 1,
IT-10125 Turin, Italy
[47]Dipartimento di Fisica, Università di Trieste and INFN, Via A. Valerio 2, IT-34127 Trieste, Italy
and Istituto di Fisica, Università di Udine, IT-33100 Udine, Italy
[48]Univ. Federal do Rio de Janeiro, C.P. 68528 Cidade Univ., Ilha do Fundão BR-21945-970 Rio de Janeiro, Brazil
[49]Department of Radiation Sciences, University of Uppsala, P.O. Box 535, SE-751 21 Uppsala, Sweden
[50]IFIC, Valencia-CSIC, and D.F.A.M.N., U. de Valencia, Avda. Dr. Moliner 50, ES-46100 Burjassot (Valencia), Spain
[51]Institut für Hochenergiephysik, Österr. Akad. d. Wissensch., Nikolsdorfergasse 18, AT-1050 Vienna, Austria
[52]Inst. Nuclear Studies and University of Warsaw, Ul. Hoza 69, PL-00681 Warsaw, Poland
[53]Fachbereich Physik, University of Wuppertal, Postfach 100 127, DE-42097 Wuppertal, Germany

1 Introduction

As long as bosonic decay channels are kinematically closed, the Standard Model (SM) Higgs boson decays preferentially into the heaviest accessible fermion pair. This leads to dominance of the $b\bar{b}$ decay mode in most of the Higgs boson mass range accessible at LEP. In extensions to the SM, however, the Higgs boson couplings to b-quarks might be suppressed. This can occur for example in the general Two Higgs Doublet Model (2HDM) [1] or in the Minimal Supersymmetric Standard Model (MSSM) [2]. Suppressed couplings to b-quarks are also possible in special composite models [3], in which the dominant Higgs boson decay channel is gluonic. The searches for the SM Higgs boson at LEP strongly rely on the identification of b-quarks to separate possible signal production from most of the backgrounds and would therefore have a reduced sensitivity to the final states predicted by such alternative models. To test these models experimentally, dedicated searches are presented, that are independent of the gluon or quark flavour into which the Higgs boson decays. Rather than stating the results in one precise theoretical framework, model-independent bounds on production cross-sections are derived that allow to test a wide class of models.

Two Higgs boson production processes are studied in this paper: the so-called Higgsstrahlung process ($e^+e^-\to hZ$) and the pair production of two Higgs bosons ($e^+e^-\to hA$), as predicted in all extensions of the Standard Model Higgs sector beyond one doublet. As usual, h denotes the lightest CP-even Higgs boson, while A is its CP-odd partner.

The paper is organized as follows. The common framework and search strategy is described in Section 2 followed by an overview of the experimental setup and the datasets in Section 3. The search for hZ production, using the fully hadronic final state, the final state with 2 jets and missing energy, and the final states with two jets and isolated leptons (electrons or muons), is described in section 4. The search for hA pair production is described in section 5. In section 6, the various analyses are combined to give flavour-independent results on the hZ and hA cross-sections, as a function of the Higgs boson mass(es). Section 7 contains the conclusions of the paper.

2 General strategy

Since the analyses presented here cannot rely on the powerful background suppression offered by b-quark identification, kinematic event information needs to be used extensively. Simultaneously, since it is intended to present results that are independent of the partonic nature of the Higgs boson decays, care must be taken not to bias the analyses towards a given flavour. The present section summarizes the procedures used to ensure this flavour-independence of the results; details for every analysis are given in the corresponding section.

To achieve good sensitivity to hZ production over a large Higgs boson mass range, from 4 GeV/c^2 up to the kinematic limit, the four-jet and missing energy channels are optimized in several domains of mass. The lepton channel however, has comparatively small background and a single analysis is sufficient to cover the whole mass range.

In the case of the search for hA production, three separate analysis streams are designed to achieve sensitivity to all event topologies, depending on the masses of the two Higgs bosons, and thereby cover a large portion of the ($m_{\rm h}$,$m_{\rm A}$)-plane (satisfying $m_{\rm h}$,$m_{\rm A}>4$ GeV/c^2, as in the hZ search).

The most efficient way to exploit the mass information of the events depends on the final states. The hZ four-jet channel and the hA analysis do not associate a single mass

to every event, because the choice of the jet pairing is not unique. A given event is thus compatible with several mass hypotheses. All events must be evaluated differently at every signal mass hypothesis, as a function of their compatibility with this hypothesis. The lepton and neutrino channels are on the contrary unambiguous, and the event information is summarized in a single estimator, independently of the signal mass hypothesis.

To ensure flavour-independence of the results, care is taken not to bias the search towards a specific hadronic decay mode of the Higgs boson. When comparing final states with quarks and gluons, sizable and competing effects arising from the different hadronization properties of quarks and gluons have to be considered. The higher multiplicity of gluon jets results in an increased selection efficiency for the gluonic final state while at the same time, mainly in the fully hadronic final states, the many additional particles induce a worse dijet mass resolution when compared to quarks, because of more frequent wrong particle to jet association.

For each final state, Higgs boson decays into gluons and quarks are evaluated, and at each Higgs boson mass hypothesis, the decay-mode resulting in the weakest expected cross-section exclusion limit in the absence of a signal is considered as the flavour-independent result. Details are given in Section 6.

Note that the differences in hadronization properties between light and heavy quarks are smaller than the differences between light quarks and gluons. In particular, the multiplicity ratio of b-quark to light quark jets is around 1.1, whereas the gluon to light-quark multiplicity ratio is around 1.4 [4]. For this reason the paper speaks of quarks without specifying their flavour. In practice, gluon jets are most often compared to light quark jets, the latter having the smallest pre-selection efficiency because of their lower average multiplicity.

In the case of heavy quarks, the energy lost in the form of escaping neutrinos from leptonic decays could in principle deteriorate the mass reconstruction when the Higgs boson(s) decays into these flavours. However, in the lepton and fully hadronic channels, the Higgs boson mass reconstruction is obtained from kinematic fits that exploit energy and momentum conservation between the initial and the final state, and the effect of the escaping neutrinos is very small. The neutrino channel, which cannot rely on these methods, needs to consider all quark flavours explicitly.

When no signal is found, upper bounds on the production cross-section times the branching fraction into hadrons are extracted for both production processes as a function of the Higgs boson masses. These bounds are expressed in terms of reference cross-sections, defined as follows. The production rate of any final state initiated by $e^+e^-\to hZ$ can be expressed in terms of the SM hZ cross-section [5]. The reference cross-section for $e^+e^-\to hA$ is obtained by computing this process in the 2HDM, in the absence of any mixing in the Higgs sector, and depends only on electroweak parameters and the h and A Higgs boson masses (the computation was performed using `HZHA` [6]). Suppression terms coming from branching fractions and possible suppression of the Higgs boson couplings to the Z (such factors are hereafter denoted by BR and R, respectively) all factorize, and are hidden in a generic (model-independent) suppression factor :

$$\begin{aligned}
\sigma_{hZ\to Z+had} &= \sigma_{hZ}^{SM} \times R_{hZ} \times BR(h \to had) \\
&\equiv \sigma_{hZ}^{SM} \times C^2_{Z(h\to had)}; \\
\sigma_{hA\to had} &= \sigma_{hA}^{ref} \times R_{hA} \times BR(h \to had) \times BR(A \to had) \\
&\equiv \sigma_{hA}^{ref} \times C^2_{hA\to had};
\end{aligned}$$

where *had* stands for hadrons. Our results will be expressed in terms of $C^2_{Z(h\to had)}$ and $C^2_{hA\to had}$.

Although the traditional CP-conserving Higgs boson nomenclature is used throughout the paper, part of the results can also be extended to the context of CP-violating Higgs sectors. For hA production, the parity and charge conjugation properties of the Higgs bosons do not play any role in the decay kinematics. The results on $C^2_{hA\to had}$ should therefore be understood as relevant to the pair production of any two Higgs bosons (i.e. $h_i h_j \to$ had), regardless of their CP properties and the Higgs bosons mass hierarchy. On the contrary, our results on $e^+e^-\to$hZ assume standard quantum numbers for the Higgs boson. Non-standard Higgs boson parity properties would imply different polarization of the associated Z boson, thereby affecting the angular distributions of the bosons and the selection efficiencies. Our results for this channel should therefore be used with care.

3 Detector, data samples and simulation

A detailed description of the DELPHI detector and the performance of its sub-systems can be found in [7]. For LEP2, the vertex detector was upgraded [8] and a set of scintillator counters (veto counters) was added to veto photons in blind regions of the electromagnetic calorimetry, at angles of 40, 90 and 140 degrees from the beam axis.

The data samples used were collected by DELPHI during the last 3 years of LEP operation (1998 to 2000), and are clustered around seven centre-of-mass energies (see Table 1). In September 2000, one of the twelve sectors of the main tracking device of DELPHI underwent an irremediable failure. The corresponding change in sensitivity has been taken into account using dedicated simulation samples.

year	1998	1999				2000	
$\sqrt{s}$ (GeV)	188.6	191.6	195.5	199.5	201.6	205.0	206.5
$\mathcal{L}$ (pb^{-1})	158.0	25.9	76.9	84.3	41.1	82.0	142.2

Table 1: *Integrated luminosities collected by the DELPHI detector at various centre-of-mass energies during the period 1998-2000.*

Background samples

For the hZ channel, two-fermion background events are simulated using the `KK2F` [9] generator, while `WPHACT` [10] is used for four-fermion final states (see [11] for the specific DELPHI implementation). For the hA analysis, prepared during an earlier stage of this work, the two-fermion and four-fermion SM backgrounds are simulated using the `PYTHIA` [12] and `EXCALIBUR` [13] generators respectively. Background from two-photon events is generated using `PYTHIA`.

hZ signal samples and data-sets

The hZ analysis uses the data from all seven centre-of-mass energies listed in Table 1. The `HZHA` generator is used to generate hZ signal samples at the centre-of-mass energies of Table 1 and at masses from 40 to 120 GeV/c^2 with a step size of 2.5 GeV/c^2. Z boson decays into quarks, neutrinos, electrons and muons are simulated, and the Higgs boson is made to decay into either a pair of gluons, or a pair of light quarks (s-quarks in practice).

The results obtained for Higgs boson decays into light quarks generalize to all quark flavours in the four-jet and lepton channels, as discussed in the previous section. For the missing energy channel, Higgs boson decays into c-quarks and b-quarks are simulated as well. Below 40 GeV/c^2, signal samples were generated every 5 GeV/c^2 in mass.

hA signal samples and data-sets

The hA analysis uses the data sets in Table 1, except for the two sets with smallest luminosities. The simulation of the hA production process also uses the `HZHA` generator in the Higgs boson mass range m_h,m_A>4 GeV/c^2 and m_h+m_A<180 GeV/c^2, using a grid of 5 GeV/c^2 if at least one of the masses is below 30 GeV/c^2 and 10 GeV/c^2 otherwise. Higgs boson decays into gluon pairs or light quark pairs are simulated, as was done for the hZ four-jet search.

4 Search for hZ production

For this search, most of the analyses used to search for a hadronically decaying Higgs boson are adapted from existing analyses set up on other subjects in DELPHI. In most cases only a brief description of the main parts in the analysis is given, and a reference is made to the publication where the analysis is described in more detail.

4.1 The fully hadronic channel

For the fully hadronic channels the Higgs mass range is divided in two regions, below and above 40 GeV/c^2, each with a dedicated analysis. This is done to cope with the changing topology when going from a heavy to a light Higgs boson mass, for which the jets from the Higgs boson decay cannot always be resolved. The final state then presents three reconstructed jets, rather than four.

Higgs boson masses above 40 GeV/c^2

The selection used to analyze the four-jet channel in the $e^+e^-\to ZZ$ cross-section measurement [14] is adapted to test the hypothesis of Higgs boson production independently of the flavour of its decay products. After a hadronic, multi jet pre-selection, the only remaining backgrounds are from ZZ and WW four-quark final states, and four jets arising from $q\bar{q}$ production with hard final state gluon radiation (hereafter denoted as $q\bar{q}(\gamma)$ events). A combined variable, P_{Higgs}, is constructed at each Higgs boson mass hypothesis to select the corresponding signal using event topology and reconstructed dijet masses.

The event topology, jet kinematics and inter-jet distances are used to distinguish between the more cigar-like $q\bar{q}(\gamma)$ events and the more spherical four-fermion events (including the hZ signal). From the reconstructed jets, a constrained fit is performed, requiring energy and momentum conservation between the initial and final state. The fitted jet-momenta are then used to extract the reconstructed dijet masses for each of the possible jet pairings. The uncertainties on the fitted momenta and their correlation matrix are taken into account in that procedure. The masses and their uncertainties are used to compute, for each event, the probability that the event is compatible with the hypotheses: WW, ZZ, $q\bar{q}(\gamma)$, or hZ with a specific Higgs boson mass. For all channels the expected dijet

mass distributions are known analytically. In the case of hZ production, the expected mass distributions change with the Higgs boson mass hypothesis so that the analysis is automatically optimal for each mass hypothesis. Finally, for each jet, the probability that it originated from a b-quark fragmentation relative to a light quark (or gluon) is computed [15]. This information is only used to enhance the sensitivity to events with a Z boson decaying into a pair of b-quarks. In the dijet assumed to originate from the Higgs boson this information is not used, thereby ensuring flavour-independence. The method employed to combine the various mass and b-tagging probabilities using likelihood ratio products is described in [14].

The number of observed events is compared in Table 2 with what is expected from background and an hZ($h\to q\bar{q}$) signal for a few Higgs boson masses, after a cut on $P_{\rm Higgs}$ chosen as to maximize the product of signal efficiency and purity. Examples of the probability distributions, when adding all data, are shown in Figure 1, for Higgs boson masses of 75, 90 and 105 GeV/c^2, respectively. The dominant background depends on the tested mass. For a 90 GeV/c^2 mass hypothesis for example, ZZ production will dominate the high purity region, while for mass hypotheses below 80 GeV/c^2 background from ZZ production is negligible.

The systematic uncertainties are dominated by the uncertainty in the modeling of the four-jet rates of $q\bar{q}(\gamma)$ processes [16]. This uncertainty is conservatively taken to be 10% over the full Higgs boson mass range. The effect of other systematics, evaluated in detail in [14], are negligible compared to this.

$m_{\rm h}$ (GeV/c^2)	$\epsilon_{\rm hZ}$(%)	hZ($h\to q\bar{q}$)	SM (no hZ)	observed
40	31.3	154.6	635.0	659
50	30.1	132.3	522.8	532
60	51.9	197.1	1784.1	1824
70	78.6	249.3	5457.3	5476
80	54.2	136.0	1681.7	1764
90	54.6	96.2	957.4	970
100	47.0	41.1	368.5	372
110	33.9	9.4	87.6	75

Table 2: Fully hadronic channel: the number of observed events compared to what is expected from background and signal ($Z\to q\bar{q}$ and $h\to q\bar{q}$, assuming a SM hZ cross-section) for a few Higgs boson masses, after a cut on $P_{\rm Higgs}$ for which the product of signal efficiency and purity is maximal. Using the combined set of simulated events at all centre-of-mass energies, the statistical uncertainties on both the signal efficiency and background level are below 1%.

At each Higgs boson mass hypothesis the distribution of $P_{\rm Higgs}$ for background and signal are used for the statistical evaluation of the compatibility of the data with the simulation, following the procedure described in [22].

Higgs boson masses below 40 GeV/c^2

Below 40 GeV/c^2 in Higgs boson mass, fully hadronic events tend to become more three-jet like, since the decay jets of the Higgs boson are not always resolved due to

the large boost. This region in mass is therefore covered by the three-jet hA analysis, described in more detail in section 5.1. Efficiencies and discriminant variable distributions are determined from hA signals with the A mass fixed to the Z mass. A few hZ samples have been simulated to verify the validity of this procedure, which was found to be correct within the systematic errors estimated in the hA three-jet channel, despite the slightly different Higgs boson angular distributions.

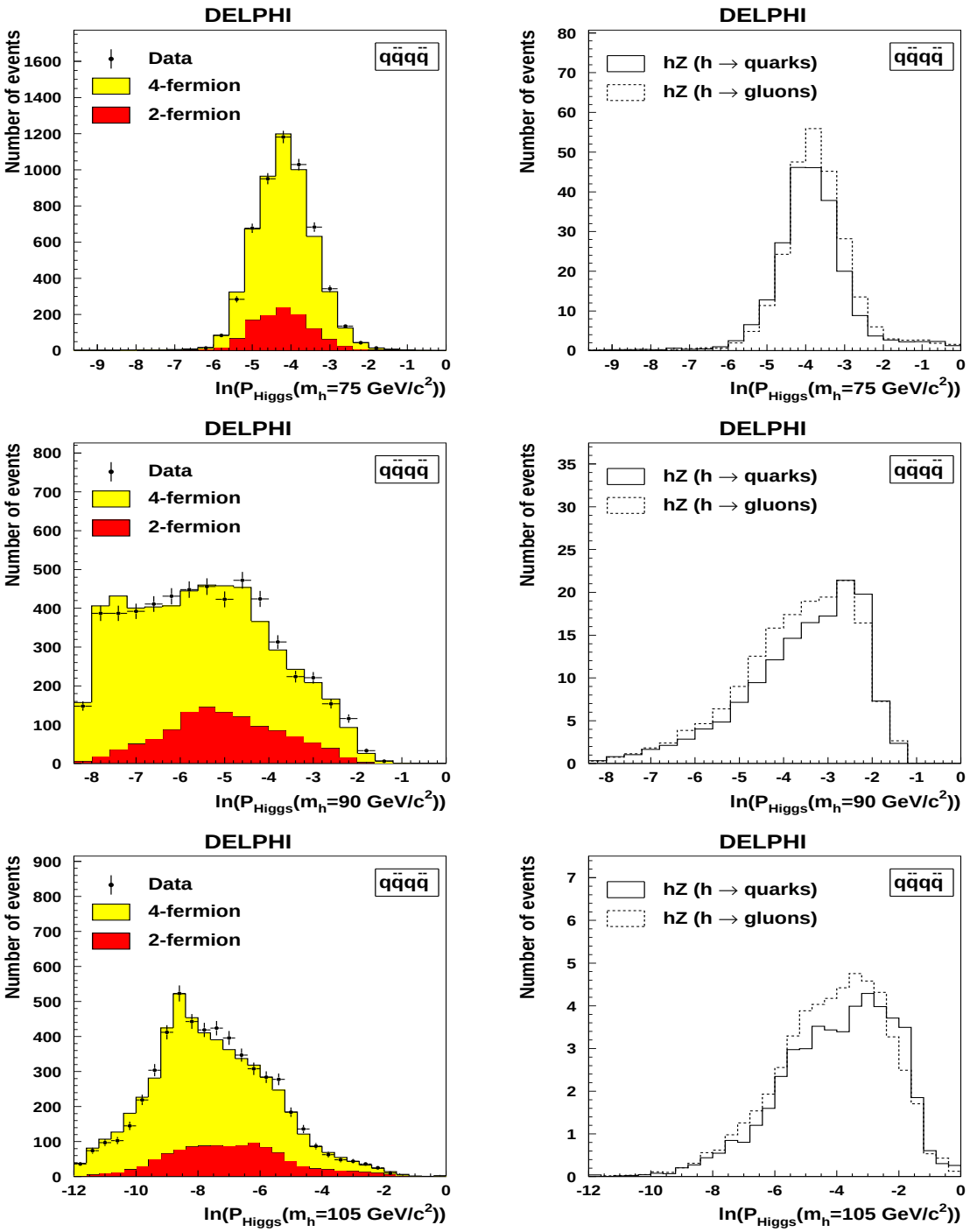

Figure 1: Distributions of the combined Higgs probabilities, P_{Higgs}, for the fully hadronic hZ final state at Higgs boson masses of 75, 90 and 105 GeV/c^2 respectively (from top to bottom). For illustrative purposes, all data from 189 to 208 GeV have been added.

4.2 The missing energy channel

The event topology in the missing energy channel changes significantly as a function of the Higgs boson mass. For Higgs masses below 40 GeV/c^2 a monojet final state is expected while for masses above 40 GeV/c^2 the jets are expected to be well separated, resulting in a two jet final state. For both topologies a dedicated analysis is constructed and is described below. As a further optimisation, the analysis for two-jet final states is optimised in three different mass regions.

4.2.1 Mono jet final states

The analysis used to measure the $Z\gamma^* \to q\bar{q}\nu\bar{\nu}$ cross-sections [20] is adopted without major modifications to test the hypothesis of low mass ($m_h < 40$ GeV/c^2) Higgs boson production in the missing energy channel with subsequent decays into hadrons of any flavour. After a pre-selection [20] to reduce background events from $\gamma\gamma$, Bhabha and $Z\gamma$ processes, three selections are designed, focussing on different expected topologies as a function of the mass of the Higgs boson.

The first selection is optimized to probe very low Higgs boson masses, using an explicit cut on the visible mass of the event, which is required to be below 6 GeV/c^2. The second selection exploits the large energy imbalance of $h\nu\bar{\nu}$ final states: events are split into two hemispheres according to the plane perpendicular to the direction of the thrust axis, and are required to have one of the hemispheres containing at least 99% of the total visible energy in the event. The third selection, which is less efficient at very low masses because of an explicit cut on the charged particle multiplicity, is mainly based on a topological requirement: events are forced into a two jet configuration and an upper cut on the opening angle of the two jets was set at 78 degrees. All three selections use the information from the veto counters, by rejecting events with hits in veto counters far away from energy depositions in calorimeters or reconstructed tracks. The three analyses are combined on an event-by-event basis, by selecting events that pass any of the three selections.

The reconstructed visible mass spectra is used as the discriminant variable for the statistical evaluation of the compatibility of the data with the simulation for different Higgs boson mass hypotheses, following the procedure described in [22]. No specific mass cuts are applied for different Higgs boson mass hypotheses. The most important remaining background sources are $Z\gamma^*$ and $We\nu$. The lefthand plot in Figure 2 shows the distribution of the reconstructed visible mass for data and background simulation. Maximum Higgs boson signal efficiencies are around 65% and dropped to 40% for masses below 5 GeV/c^2 and above 40 GeV/c^2 as can be seen in the righthand plot of Figure 2.

The systematic uncertainty on the predicted background level for this final state is 9%, obtained by changing the various selection criteria within their uncertainties, taking into account the effects from the differences between data and simulation in kinematic distributions relevant for the analysis. The uncertainty also includes a 5% contribution from the statistical uncertainty on the simulated background sample [20]). The uncertainty on the signal selection efficiency, estimated by using different simulation programs, is 5%.

4.2.2 Two jet final states

The search for events with two jets and missing energy, compatible with a Z boson decaying into two neutrinos, follows closely the analysis applied to search for an invisibly

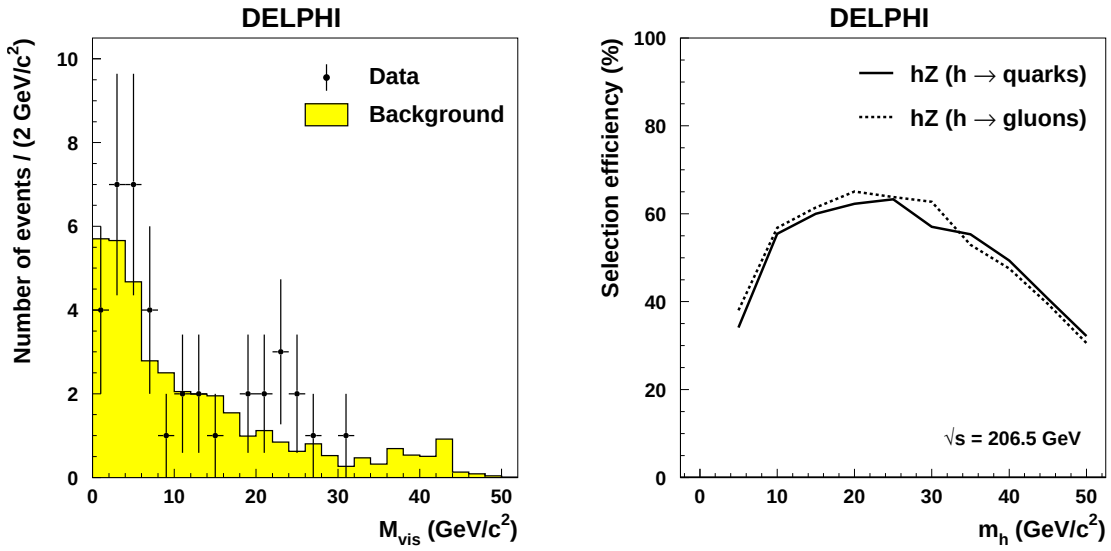

Figure 2: The lefthand plot shows the distribution of the invariant mass of the hadronic system after the $q\bar{q}\nu\bar{\nu}$ event selection. Dots stand for data while the solid histogram describes the expected background. For illustrative purposes, all data from 189 to 208 GeV have been added. In the righthand plot the selection efficiency is shown as a function of the mass of the Higgs boson at the highest centre-of-mass energy.

decaying Higgs boson produced together with a Z boson that decays into hadrons as described in [17]. To obtain a good performance over the whole mass range from 40 to 115 GeV/c^2, three mass windows (low, intermediate and high) are defined and each is treated with a dedicated analysis. To reduce background originating from $q\bar{q}(\gamma)$ and $\gamma\gamma$ processes, a common pre-selection is applied as described in [17], followed by the rejection of events with more than two identified leptons. After this step, two jets are reconstructed from all particles in the event using the DURHAM clustering algorithm. The final discrimination is achieved in the three analysis streams with an Iterative Discriminant Analysis (IDA) [18], using two steps. After the first IDA step, a cut on the IDA output is made to remove a large part of the background while retaining 90% of the signal. The IDA is then retrained on the events passing this selection. To ensure flavour-independence, the IDA is trained simultaneously on $s\bar{s}$, $c\bar{c}$ and $b\bar{b}$ flavours, resulting in a comparable performance for all flavours.

Low mass analysis

In the low mass analysis, twelve variables are used to obtain a highly discriminant IDA output. These are: the scalar and vector sum of all reconstructed particles' momenta, projected in the transverse plane; the visible energy; the thrust of the event; the energy of the least energetic jet in the three-jet configuration; the difference between the Fox-Wolfram moments H2 and H4 [19]; the energy and the momentum of the most isolated particle; the opening angle of the two jet axes; the angle between the plane formed by the two jet axes and the beam axis; the missing mass and the highest transverse momentum of a particle with respect to its jet. The IDA was trained over the whole mass range from 40 to 67.5 GeV/c^2.

Intermediate mass analysis

The analysis in the intermediate mass range uses the same twelve variables as in the low mass analysis, except for the energy of the least energetic jet in the three-jet configuration, which is replaced by the event b-tag probability as defined in [15]. Also in this analysis the IDA has been trained over the whole mass range from 70 to 87.5 GeV/c^2.

High mass analysis

The same twelve variables as in the intermediate mass analyses are used in the high mass analysis, although with slightly different selections cuts that remove the tails in the input distributions to the IDA. To avoid training on events beyond the kinematical limit of the hZ process, the mass range for the training of the IDA has been varied for the different centre-of-mass energies. The mass range is from 92.5 to 97.5 GeV/c^2 for 188.6 GeV data, from 92.5 to 107.5 GeV/c^2 for 191.6 to 201.6 GeV data and finally, from 92.5 to 115 GeV/c^2 for 205 to 206.5 GeV data.

Mass reconstruction and the final discriminant variable

The mass of the dijet system, which corresponds to the mass of the Higgs boson, is computed with a Z-mass constraint for the missing mass as in [17]. The distribution of the reconstructed Higgs boson mass for background and signal events is used, for each Higgs boson mass hypothesis separately, to select candidate events from within a mass window that is optimized to maximize the product of efficiency and purity.

The agreement between data and simulations at this stage is illustrated in Table 3 which compares the number of observed events with what is expected from background and signal ($h\to q\bar{q}$) at a few Higgs boson masses.

The discriminant variable computed in the second step of the IDA after this mass selection is used as the final discriminating variable. The distributions of the IDA variable after the second iteration are shown in Figure 3 for data, background and signal events, for three different Higgs boson mass hypotheses, namely 75, 90 and 105 GeV/c^2, and combining all data. In that figure it is also shown that, although the resolution on the two jet invariant mass is worse for gluonic Higgs boson decays than for quark decays, the large charged track multiplicity in signal events from $h\to gg$ results in a better separation between background and signal for gluon decays.

Systematics

The estimation of the systematic uncertainties also follows closely what was done in the search for invisible Higgs boson decays [17]. The dominant contribution originates from uncertainties in the description of the energy flow reconstruction, which is important for the estimation of the $q\bar{q}(\gamma)$ background. Calibration data taken at a centre-of-mass energy close to the Z-pole are used to evaluate these systematics using a method described in [14,17]. The effect on the background varies from year to year due to different detector operating conditions such as imperfect calibration and alignment. The uncertainties are in the range of 5.7% to 12.6% for the low mass analysis, 6.2% to 10.2% for the intermediate mass range and 4.0% to 8.2% for the high mass range, depending on the centre-of-mass energy. Compared to these, the uncertainties on the background level due to the choice of jet clustering algorithm and the b-tagging procedure are very small.

m_h (GeV/c^2)	ϵ_{hZ}(%)	hZ(h→q$\bar{q}$)	SM(no hZ)	observed
40	44.1	62.4	5.5	6
50	40.7	51.2	8.7	8
60	39.7	43.1	16.2	18
70	43.0	39.0	82.8	72
80	45.8	32.9	165.2	155
90	50.6	25.5	257.9	238
100	44.6	11.2	121.4	124
110	42.0	3.3	66.9	76

Table 3: Missing energy channel, two jet final state: the number of observed events compared to what is expected from background and signal (Z→$\nu\bar{\nu}$ and h→q$\bar{q}$, assuming a SM hZ cross-section) for a few Higgs boson masses after a set of mass cuts to optimize the separating power for each tested Higgs boson mass. Using the combined set of simulated events at all centre-of-mass energies, the statistical uncertainties on both the signal efficiency and background level are below 1%.

The total systematic error on the signal efficiency coming from jet clustering, b-tagging and the mismodelling of the energy flow is between 1 and 3% with the largest error for the low mass analysis.

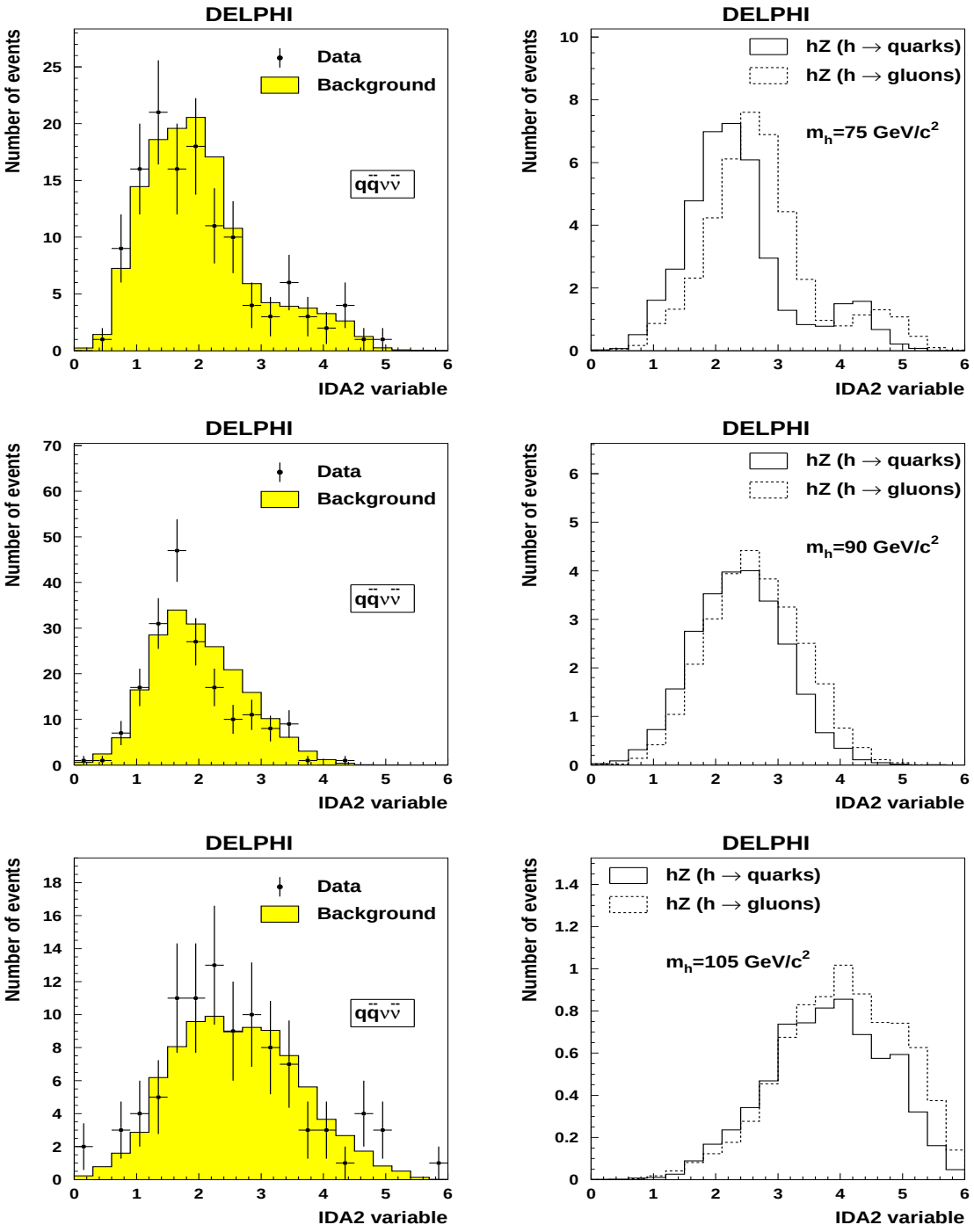

Figure 3: Distributions of the discriminant variables used in the missing energy channel, after a set of mass cuts optimized to maximize the separating power for each Higgs boson mass hypothesis The distributions shown here correspond to Higgs boson mass hypotheses of 75, 90 and 105 GeV/c^2 from top to bottom respectively. For illustrative purposes, all data from 189 to 208 GeV have been added.

4.3 Two jets and a pair of isolated leptons

The $q\bar{q}e^+e^-$ and $q\bar{q}\mu^+\mu^-$ channels are analysed in the same way as in the $e^+e^- \rightarrow ZZ$, $Z\gamma^*$ cross-section measurements [14,20]. Events are selected by sequential cuts, initially without explicit conditions on the invariant mass of the leptonic or hadronic system. The particle identification criteria were carefully tuned to maximize the efficiency of selecting leptons and the signal to background ratio.

The final discriminating variable for the statistical evaluation of the compatibility of the data with the simulation, following the procedure described in [22], is the reconstructed mass of the hadronic system after different mass cuts to enhance the possible contribution of the hZ signal. These mass cuts take into account both the varying mass resolution of the signal and the changing background level from the ZZ and $Z\gamma^*$ processes that dominate these topologies.

The distribution of the reconstructed mass of the hadronic pair when the mass of the lepton pair is within 15 GeV/c^2 of the Z mass is shown in Figure 4 for the $q\bar{q}e^+e^-$ and $q\bar{q}\mu^+\mu^-$ channels separately. In Tables 4 and 5, the signal efficiencies for these channels are displayed and the number of observed events is compared to what is expected from background and from $h \rightarrow q\bar{q}$ signals.

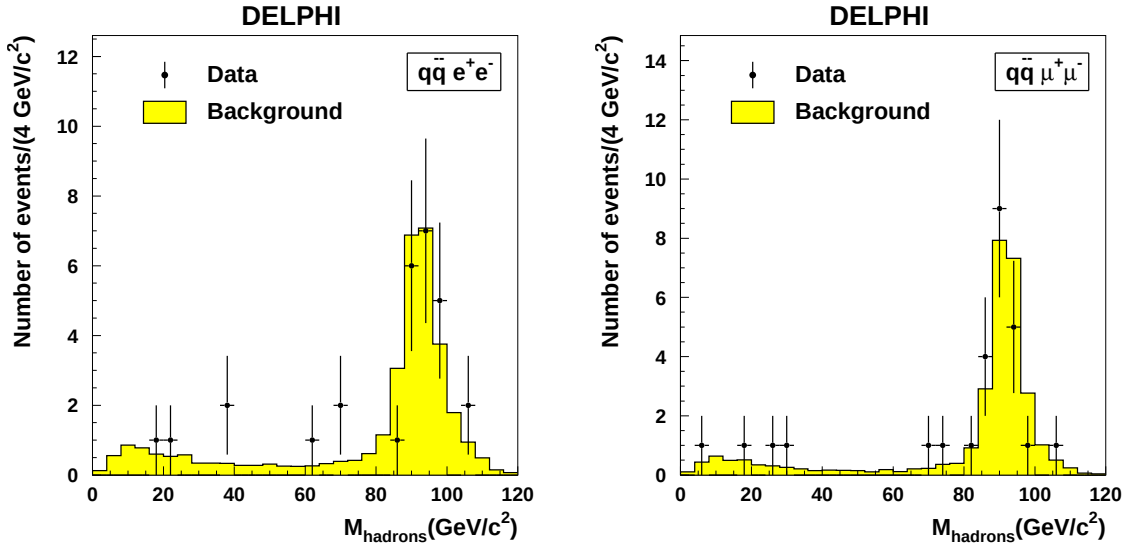

Figure 4: Distribution of the reconstructed mass of the hadronic pair when the mass of the lepton pair is within 15 GeV/c^2 of the Z mass. The left(right) plot represents the $q\bar{q}e^+e^-$($q\bar{q}\mu^+\mu^-$) channel. For illustrative purposes, all data from 189 to 208 GeV have been added.

The systematic uncertainties that are considered include the uncertainty in the lepton identification and the uncertainty on the signal selection efficiency. Combined with the statistical uncertainty on the simulated sample, these effects result in a relative systematic uncertainty in selecting $q\bar{q}e^+e^-$ and $q\bar{q}\mu^+\mu^-$ events of 5%. The uncertainty on the small residual background rate is dominated by the MC statistics and amounts to 15%.

5 Search for hA production

The search for hA production in the flavour-independent hypothesis is designed to cover a large part of the kinematically accessible h and A mass range, and is based on general kinematic features such as event shapes and detailed mass information. Again, the significantly higher multiplicity in gluon decays results in a higher selection efficiency for the gluon final state, but also results in a worse mass resolution when compared to quark jets. To minimize biases that may arise from these competing effects, the selection efficiencies are determined using hA $\rightarrow$ light quarks samples, while the mass resolution is evaluated with samples of hA $\rightarrow$ gluons.

5.1 Analysis streams

A first pre-selection is applied to all events, requiring at least 20 charged particle tracks, a total reconstructed energy greater than 60% of the centre-of-mass energy, and an effective centre-of-mass energy after initial state radiation [23] greater than 150 GeV. The efficiencies of the multiplicity cut are typically 98% for the hA $\rightarrow$ light quarks signal samples, and 100% for the hA $\rightarrow$ gluons samples. In the rest of the analysis, it is necessary to consider separately three different sets of criteria, to achieve good performance over a large range in the (m_{h},m_{A})-plane, as described below.

Four jets

Close to the kinematic limit and when both Higgs bosons have comparable masses, a four-jet topology is expected. To analyse this topology, events are clustered into four jets with the DURHAM algorithm [21]. All jets are required to have an invariant mass larger than 2 GeV/c^2, and to contain at least two charged particles. Events are retained in this stream if their thrust is below 0.85 and if the product of the smallest jet energy and inter-jet angle (called $\mathrm{E_{min}}\alpha_{\mathrm{min}}$) is greater than 10 GeV·rad. Dijet invariant mass information is used to reject events compatible with WW production as in [14], requiring the corresponding probability, called $\mathrm{P_{WW}}$, to be less than 0.01. This proves helpful not only in the case of $m_{\mathrm{h}} = m_{\mathrm{A}} \sim 80$ GeV/c^2 but also for other masses, where WW production contributes to the expected background through wrong jet pairings.

Three jets

With increasing mass difference between the h and the A, the events tend to become more three jet-like, since the decay jets of the lighter Higgs boson cannot always be resolved. The same behavior is observed if h and A both have low masses, because of the larger boost in this case. To analyse this topology, only events with thrust values between 0.70 and 0.92 are kept. Events are then clustered into four jets, and the compatibility with WW production is tested as in the four-jet stream. The remaining events are clustered into three jets. As before, all jets are required to have a mass larger than 2 GeV/c^2 and to contain at least two charged particles.

Three jets with high thrust

Finally, if both Higgs bosons are very light (below 30 to 40 GeV/c^2), signal events tend to become cigar-like. Events are selected in this analysis stream if they have a thrust $\geq$ 0.92, and are clustered into three jets, each jet having to satisfy the same quality criteria

as above. As the dominant background comes from two-quark processes the kinematic compatibility with W-pair events is not tested.

Distributions of the variables used (thrust, $E_{min}\alpha_{min}$ and P_{WW}) are shown in Figure 5 for signal masses relevant to these three analysis streams. Their performances and complementarity are illustrated in Table 6, where mass-averaged efficiencies, obtained for the different categories of signal events, are summarised. As discussed above, these efficiencies are obtained assuming h and A decays into light quarks. From comparisons with a number of signal samples assuming b-quark decays of the Higgs bosons, the quark flavour-dependence of the efficiencies is smaller than 2%. The efficiencies obtained with gluonic Higgs boson decays are higher by a factor up to 1.2 in the three jet and four jet analyses, and by a factor up to 2 in the high thrust analysis. The numbers of observed data and expected background events are shown in Table 7.

5.2 Final discriminant variable

In all three analysis streams, a four-constraint fit is performed on the selected events, requiring total energy and momentum conservation. A discriminant variable is then built from the reconstructed jet and dijet masses and their errors, by minimising the following quantity:

$$\chi^2(m_{1,test}, m_{2,test}) = \left(\frac{m_{1,rec} - m_{1,test}}{\delta m_{1,rec}}\right)^2 + \left(\frac{m_{2,rec} - m_{2,test}}{\delta m_{2,rec}}\right)^2,$$

defined for each event, over all possible pairing combinations. In the above expression, $m_{1,rec}$ is the mass of a given dijet, $m_{2,rec}$ is the mass of the opposite dijet in the four-jet stream, and of the opposite jet in the other streams, and $\delta m_{1,2}$ are the corresponding errors as obtained from the kinematic fit. This discriminant variable is computed for data and background, for each test mass configuration $(m_{1,test}, m_{2,test})$, on a 1×1 GeV/c^2 grid in the (m_h,m_A)-plane and projected into histograms as illustrated in Figure 6. The range and bin size of the histograms is the same for all analysis streams and mass configurations.These histograms are used for the statistical evaluation of the compatibility of the data with the simulation, following the procedure described in [22].

To determine the shape of the signal distributions at mass configurations that are not simulated, the histograms are linearly interpolated, bin by bin, between the three closest simulated points. This procedure is adopted in this particular case, because the discriminant variable is designed to have a slowly varying distribution for the signal as a function the signal mass. The validity of this procedure is demonstrated in section 5.3.

5.3 Systematic uncertainties

Sources of systematic uncertainties affecting this analysis are related to imperfect simulation of the detector and of SM processes, to residual flavour-dependence of the selections, and to the signal interpolation procedure. All effects are discussed below.

The numerical differences at preselection level between the observed data and the expectation from SM processes are taken as a first contribution to the uncertainty on the background prediction. For every subsequent selection variable, the difference of the average values of the corresponding distributions in data and simulation is computed;

the selection cut is then varied by an amount given by this difference. This procedure leads to an estimated systematic uncertainty on the backgrounds of 5% in the four-jet and three-jet streams, and 10% in the high-thrust stream. The higher uncertainty in this stream is mainly due to the observed numerical discrepancy after the preselection.

As stated earlier, the flavour-dependence of the selection efficiencies is estimated by comparing the results obtained for gluon decays, light quark decays, and b-quark decays. The pre-selection efficiency is slightly worse (by at most 2%) in the case of light quark decays, and is applied to the gluon decays as well. The remaining selections have a flavour-dependence of less than 2%. This number is taken as a contribution to the systematic uncertainty on the signal rate.

The lefthand plot of Fig. 7 shows a comparison of a simulated distribution with the one that was obtained by interpolating between two neighbouring generated points. The shapes are well reproduced. To quantify more precisely what accuracy can be expected from this procedure, the previous exercise is repeated on a large number of simulated mass configurations. In each case, the bin contents of the simulated and interpolated histograms are compared. The distribution of the true-to-interpolated bin content ratio has a spread of 5%, which is taken as a second contribution to the systematic uncertainty on the signal rate. Note that this is a conservative estimate as the real interpolation is over smaller intervals than the 20 GeV/c^2 used in the estimate.

Finally, the righthand plot of Figure 7 shows the probability density function of the discriminant variable obtained for quarks and gluons, at the mass point (110,30). As expected, a worse mass resolution on gluon jets translates into a somewhat reduced discriminating power (this is true for all mass points). The present analysis, with a pre-selection determined on light-quark signal samples and a kinematic analysis calibrated on gluon samples, thus has no bias towards a given flavour that would invalidate the results when considering other hadronic decays of the Higgs bosons.

6 Results

Results from the different analyses and topologies have been combined, and the statistical compatibility of the data with a possible Higgs boson signal has been evaluated using the likelihood ratio technique [22] that was also used in other Higgs boson searches in DELPHI (see ref. [24] for an example). The inputs to this procedure from all channels and analyses are constructed for each of the simulated Higgs boson mass hypotheses. During the fine scan over all Higgs boson mass hypotheses, the inputs corresponding to the nearest simulation point are used, where the signal level is scaled to the correct SM signal cross-section for this particular Higgs boson mass, and the various confidence levels are then computed by changing the hZ cross-section with respect to its SM value (see Section 2). The inputs from all channels are quickly reviewed for the hZ and hA analyses separately in the next sections. Over the whole studied mass range the natural width of the Higgs boson is assumed to be much smaller than the resolution on the reconstructed mass ($\sim$ 1-3 GeV/c^2).

No evidence for Higgs boson production has been observed and results are presented in terms of excluded cross-sections (at 95% confidence level) as a function of the Higgs boson masses. The results are presented separately for hZ and hA production both with direct decays of the Higgs bosons into hadrons.

6.1 Excluded cross-sections for hZ production

At each simulated Higgs boson mass hypothesis, the inputs from the various channels to the likelihood analysis have been constructed. For masses below 40 GeV/c^2 the fully hadronic channel provides the distribution of its discriminant variable, $\chi^2(\mathrm{m}_1, \mathrm{m}_2)$, for background simulation and hZ signal (as shown in Fig.1), while for the missing energy channel there is no discriminant variable, and only the number of expected events from background and the hZ signal are provided for each Higgs boson mass hypothesis. For masses above 40 GeV/c^2 two analyses provide the distribution of a discriminant variable for background and signal: the distribution of $\mathrm{P}_{\mathrm{Higgs}}(\mathrm{m_h})$ for the fully hadronic channel (as shown in Fig.6) and the distribution of the second IDA output after a set of mass cuts for the missing energy channel(see Figure 3). The final state with two jets and a pair of isolated leptons provides for each mass hypothesis the number of expected events from background and the hZ signal.

Cross-section limits have been computed for Higgs boson decays into either gluon or quark pairs and the flavour-independent result at each mass is then given by the weakest exclusion. For masses above 40 GeV/c^2, the quark pair result provides the most conservative exclusion. The transition between the hZ fully hadronic and the hZ three-jet analysis and between the two missing energy channels is at m_{h}=40 GeV/c^2, a mass where the performance of these channels is comparable. In Figure 8 the excluded cross-section for a Higgs boson with purely hadronic decays is shown, normalised to the SM cross-section. Observed and expected limits agree well over a wide range of masses. The largest discrepancy occurs for a Higgs boson mass close to 30 GeV/c^2 where an excess of 2.65 σ is observed (the excess is around 2.5 σ when the result is averaged over the mass resolution at that particular Higgs boson mass hypothesis). The excess is shared by two channels: the missing energy channel contributes around 2 σ, and the low-mass fully hadronic channel contributes around 1.5 σ. Checks that have been performed on the jet angular distributions do not favour a signal interpretation of the excess. The confidence level in the background hypothesis is shown in Figure 9.

Table 8 gives the mass limits for a Higgs boson with a SM production cross-section which exclusively decays into either quark or gluon pairs and, as a comparison, the results achieved in the SM Higgs boson searches [24].

6.2 Excluded cross-sections for hA production

At each simulated Higgs boson mass hypothesis, the inputs to the likelihood analysis are constructed using the distribution of the discriminant variable, $\chi^2(\mathrm{m}_1, \mathrm{m}_2)$, for background simulation and hZ signal as shown in Figure 6. The three different hA analysis streams have been combined to search for Higgs boson pair production. The three-jet stream and the high-thrust stream are statistically independent and are combined as such in the result derivation. The overlap between these selections and the four-jet stream is solved by choosing the strongest expected exclusion performance for each mass point.

No evidence for signal was observed. Figure 10 displays regions excluded at the 95% CL in the (m_{h},m_{A})-plane, for a few fixed values of $C^2_{hA\to had}$. When both Higgs boson masses are comparable and when the production cross-section is maximal, the combinations with m_{h}+m_{A}below $\sim$140 GeV/c^2 are excluded. When one of the Higgs boson is very light, the mass of the other boson is constrained to be either below 4 GeV/c^2, the threshold of hA searches, or above 108 GeV/c^2, in the case $C^2_{hA\to had} = 1$. The 3-jet and high-thrust

analysis streams allow a significant portion of the mass plane to be excluded even when the production cross-section is smaller than 25% of the maximal rate.

These results are valid in the case of direct Higgs boson decays into hadrons. When the intermediate h→AA decay mode opens (the corresponding kinematic domain is illustrated by the dashed lines in Figure 10), the six-parton final state may become dominant. The sensitivity of the present analyses to this topology has not been evaluated.

As stated in the introduction, the hA exclusions are valid independently of the parity properties of h and A, and in particular may be interpreted in the context of a CP-violating Higgs sector.

7 Summary

DELPHI used LEP2 data to search for Higgs bosons with hadronic decays of any flavour. No signal has been found in either of the two main production mechanisms ($e^+e^-\to Z^* \to hZ$ and $e^+e^-\to Z^* \to hA$) studied, in a broad range of masses extending from 4 GeV/c^2 to close to the kinematic limit.

For the hZ process, cross-sections larger than about 10-60% of the expected SM values have been excluded in the range of masses from 4 to 100 GeV/c^2, independent of the flavour of the Higgs boson decays. Under the assumption of a production cross-section equal to that in the SM, observed and expected lower mass limits at the 95% CL of 108.0 GeV/c^2 and 110.6 GeV/c^2 have been obtained, respectively.

For the hA process, a large part of the available mass range have been excluded, independent of the flavour of the Higgs boson decays. In the case of full production strength and 100% branching fraction into hadrons (i.e. $C^2_{hA\to had} = 1$), the excluded region extends roughly up to $m_{h,A}$= 108 GeV/c^2 for the heavier Higgs boson, when the lighter one has a mass below 10 GeV/c^2. When both masses are equal, $m_{h,A} < 70$ GeV/c^2 is excluded. Even for reduced cross-sections, significant portions of the mass plane remain excluded.

Acknowledgements

We are greatly indebted to our technical collaborators, to the members of the CERN-SL Division for the excellent performance of the LEP collider, and to the funding agencies for their support in building and operating the DELPHI detector.
We acknowledge in particular the support of
Austrian Federal Ministry of Education, Science and Culture, GZ 616.364/2-III/2a/98,
FNRS–FWO, Flanders Institute to encourage scientific and technological research in the industry (IWT), Federal Office for Scientific, Technical and Cultural affairs (OSTC), Belgium,
FINEP, CNPq, CAPES, FUJB and FAPERJ, Brazil,
Czech Ministry of Industry and Trade, GA CR 202/99/1362,
Commission of the European Communities (DG XII),
Direction des Sciences de la Matière, CEA, France,
Bundesministerium für Bildung, Wissenschaft, Forschung und Technologie, Germany,
General Secretariat for Research and Technology, Greece,
National Science Foundation (NWO) and Foundation for Research on Matter (FOM), The Netherlands,
Norwegian Research Council,
State Committee for Scientific Research, Poland, SPUB-M/CERN/PO3/DZ296/2000, SPUB-M/CERN/PO3/DZ297/2000 and 2P03B 104 19 and 2P03B 69 23(2002-2004)
JNICT–Junta Nacional de Investigação Científica e Tecnológica, Portugal,
Vedecka grantova agentura MS SR, Slovakia, Nr. 95/5195/134,
Ministry of Science and Technology of the Republic of Slovenia,
CICYT, Spain, AEN99-0950 and AEN99-0761,
The Swedish Natural Science Research Council,
Particle Physics and Astronomy Research Council, UK,
Department of Energy, USA, DE-FG02-01ER41155,
EEC RTN contract HPRN-CT-00292-2002.

References

[1] J. F. Gunion, H. E Haber, G. L. Kane and S. Dawson, *The Higgs Hunter's Guide*, Addison-Wesley Publishing Company, 1990.

[2] M. Carena, S. Heinemeyer, C. E. M. Wagner and G. Weiglein, *Suggestions for improved benchmark scenarios for Higgs-boson searches at LEP2*, hep-ph/9912223;
M. Carena, S. Mrenna and C. E. M. Wagner, Phys. Rev. D**60** (1999) 075010;
W. Loinaz and J. D. Wells, Phys. Lett. B**445** (1998) 178;
M. Carena, J. Ellis, A. Pilaftsis and C. E. M. Wagner Nucl. Phys. **B586** (2000) 92.

[3] X. Calmet and H. Fritzsch, Phys. Lett. **B496** (2000) 190.

[4] DELPHI Collaboration, P. Abreu *et al.*, Phys. Lett. **B449** (1999) 383.

[5] E. Gross, G. Wolf and B. Kniehl, Z. Phys. **C63** (1994) 417;
Erratum Z. Phys. **C66** (1995) 321;

[6] P. Janot, in CERN Report 96-01, Vol. 2, p. 309.

[7] DELPHI Collaboration, P. Abreu *et al.*, Nucl. Instr. and Meth. **A378** (1996) 57; DELPHI Collaboration, P. Aarnio *et al.*, Nucl. Instr. and Meth. **A303** (1991) 233.
[8] P. Chochula *et al.* (DELPHI Silicon Tracker Group), Nucl. Instr. and Meth. **A412** (1998) 304.
[9] S. Jadach, B. F. L. Ward and Z. Was, Comp. Phys. Comm. **130** (2000) 260.
[10] E. Accomando and A. Ballestrero, Comp. Phys. Comm. **99** (1997) 270; E. Accomando, A. Ballestrero and E. Maina, Comp. Phys. Comm. **150** (2003) 166.
[11] A. Ballestrero *et al.*, Comp. Phys. Comm. **152** (2003) 175.
[12] T. Sjöstrand *et al.*, Comp. Phys. Comm. **135** (2001) 238.
[13] F. A. Berends, R. Pittau and R. Kleiss, Comp. Phys. Comm. **85** (1995) 437.
[14] DELPHI Collaboration, J. Abdallah *et al.*, Eur. Phys. J. C **30** (2003) 447.
[15] DELPHI Collaboration, J. Abdallah *et al.*, *b-tagging in DELPHI at LEP* CERN-EP/2002-088 (Submitted to Eur. Phys. J. C).
[16] A. Ballestrero *et al.*, CERN-EP/2000-009 (2000), p. 137.
[17] DELPHI Collaboration, J. Abdallah *et al.*, *Searches for invisibly decaying Higgs bosons with the DELPHI detector at LEP* CERN-EP/2003-046 (Submitted to Eur. Phys. J. C).
[18] T. G. M. Malmgren, Comp. Phys. Comm. **106** (1997) 230; T. G. M. Malmgren and K. E. Johansson, Nucl. Instr. and Meth. **A403** (1998) 481.
[19] G. C. Fox and S. Wolfram, Nucl. Phys. **B149** (1979) 413.
[20] DELPHI Collaboration, J. Abdallah *et al.*, *$Z\gamma^*$ production in e^+e^- interactions at $\sqrt{s}$ = 183-209 GeV* (To be submitted to Eur. Phys. J. C).
[21] S. Catani *et al.*, Phys. Lett. **B269** (1991) 432; N. Brown, W. J. Stirling, Z. Phys. **C53** (1992) 629.
[22] A. L. Read, in CERN Report 2000-005, p. 81 (2000).
[23] P. Abreu *et al.*, Nucl. Instr. and Meth. **A427** (1999) 487.
[24] DELPHI Collaboration, J. Abdallah *et al.*, *Final results from DELPHI on the searches for SM and MSSM Neutral Higgs bosons* CERN-EP/2003-008 (Submitted to Eur. Phys. J. C).

m_h (GeV/c^2)	ϵ_{hZ}(%)	hZ(h→q$\bar{q}$)	SM(no hZ)	observed
40	59.8	14.2	1.6	3
50	61.8	12.9	1.1	2
60	63.3	11.4	1.5	3
70	63.4	9.5	2.3	4
80	66.1	7.9	17.6	18
90	69.5	5.8	23.3	18
100	68.2	2.8	16.3	11
110	64.2	0.8	1.9	3

Table 4: Final state with two jets and a pair of isolated electrons: the number of observed events with electrons in the final state compared with the expectation from background and signal (Z→e^+e^- and h→q$\bar{q}$, assuming a SM hZ cross-section) for a few Higgs boson masses, after the mass cuts that maximize the separating power for each tested Higgs boson mass.

m_h (GeV/c^2)	ϵ_{hZ}(%)	hZ(h→q$\bar{q}$)	SM(no hZ)	observed
40	77.1	18.1	1.5	3
50	77.5	16.1	2.3	4
60	78.5	14.1	2.0	3
70	76.8	11.5	3.3	3
80	78.0	9.3	20.0	16
90	80.6	6.7	25.6	20
100	81.1	3.3	17.8	18
110	76.8	0.9	3.1	2

Table 5: Final state with two jets and a pair of isolated muons: the number of observed events with muons in the final state compared with the expectation from background and signal (Z→$\mu^+\mu^-$ and h→q$\bar{q}$, assuming a SM hZ cross-section) for a few Higgs boson masses, after the mass cuts that maximize the separating power for each tested Higgs boson mass.

	ϵ_{hA}(%)(four-jet)	ϵ_{hA}(%)(three-jet)	ϵ_{hA}(%)(high-thrust)
four-jet events	$\sim$ 70	$\sim$ 45	0-5
three-jet events	$\sim$ 50	$\sim$ 70	0-5
high-thrust events	0-5	0-5	10-15

Table 6: Efficiencies of the three analysis streams in the hA search applied to three classes of signal events, defined as: *Four-jet*: both m_h and $m_A > 60$ GeV/c^2; *high-thrust*: both m_h and $m_A < 30$ GeV/c^2; *three-jet*: remaining cases.

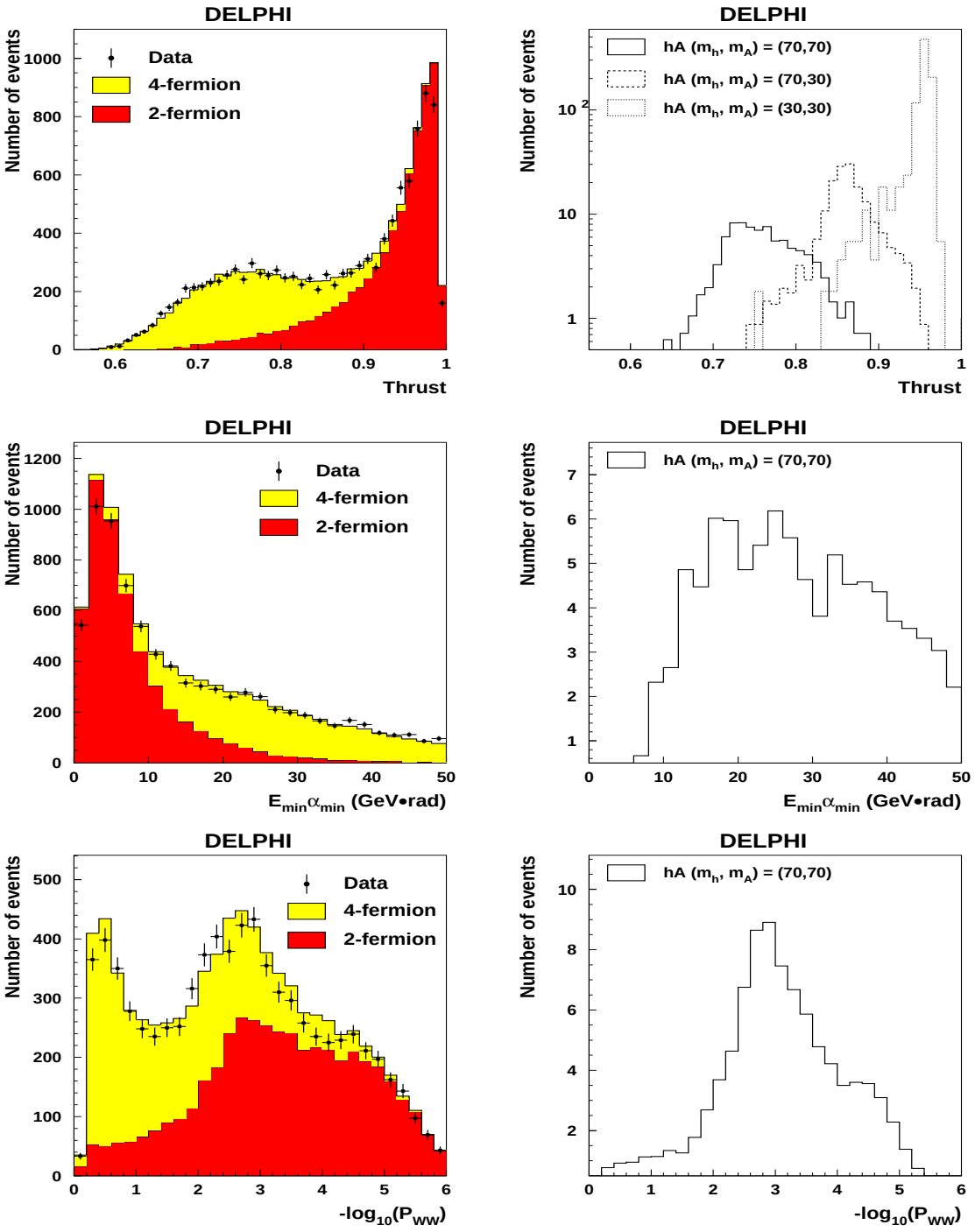

Figure 5: hA search: data to Monte Carlo comparisons at the pre-selection level, for the variables used in the three selection streams. In the right part, the dots represent the data, the light(dark) histogram corresponds to the expected four-fermion(two-fermion) background. The top plots display the thrust distributions, and how they differ for various signal mass hypotheses. The middle and bottom plots show respectively $E_{min}\alpha_{min}$, which is used in the four-jet stream and the variable $-\log_{10}(P_{WW})$, used in both the four-jet and the three-jet stream. The discriminating power is indicated by showing the distributions from representative signal samples.

centre-of-mass energy	189 GeV	196 GeV	200 GeV	>204.5 GeV
four-jet stream :				
expected background	433.5	221.3	259.0	634.5
observed events	459	248	232	642
three-jet stream :				
expected background	1593.3	750.6	797.0	1894.3
observed events	1585	736	772	1824
high-thrust stream :				
expected background	1384.9	642.5	654.3	1516.3
observed events	1331	612	607	1450

Table 7: Numbers of observed events and expected background in the hA search summed over all considered data-sets, and for each analysis stream. The statistical uncertainty on the background estimates is 2%.

	expected lower limit (GeV/c^2)	observed lower limit (GeV/c^2)
DELPHI ($h \to q\bar{q}$)	108.0	110.6
DELPHI ($h \to gg$)	109.2	111.0
DELPHI (SM decay)	113.3	114.1

Table 8: The expected and observed 95% CL lower limits (in GeV/c^2) on the mass of a hadronically decaying Higgs boson, assuming its cross-section is identical to that in the SM. The results of the SM Higgs boson search are also given for comparison.

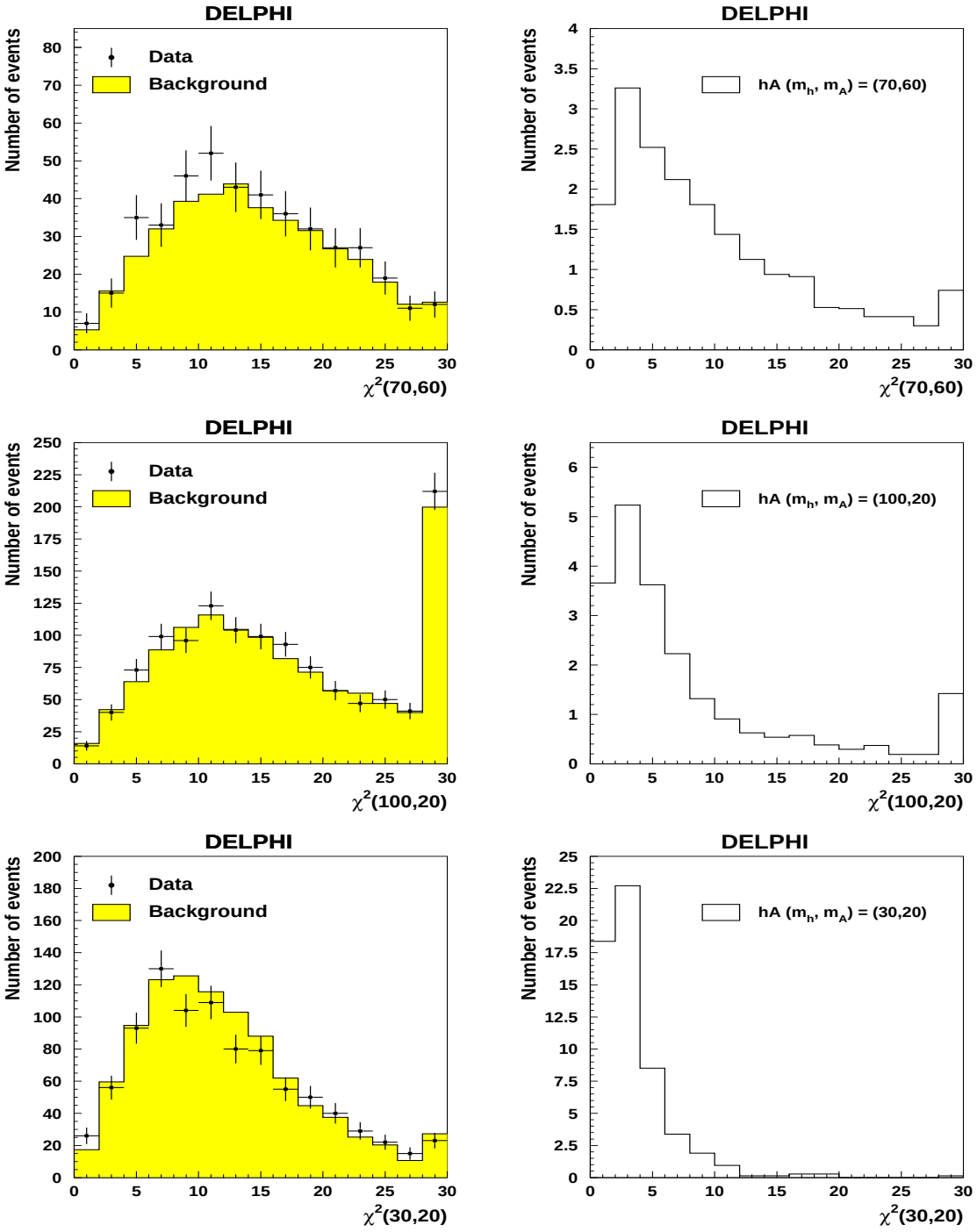

Figure 6: hA search: distributions of the variable $\chi^2(m_1, m_2)$ for the data and expected background (left) and signals (right). The upper plots show the discrimination obtained for a (m_{h},m_{A}) = (70,60) hypothesis in the four-jet stream. The central plots show the discrimination obtained for a (m_{h},m_{A}) = (100,20) hypothesis, in the three-jet stream. The lower plots show the discrimination obtained for a (m_{h},m_{A}) = (30,20) hypothesis, in the high-thrust stream. In each distribution, overflows have been included in the last bin.

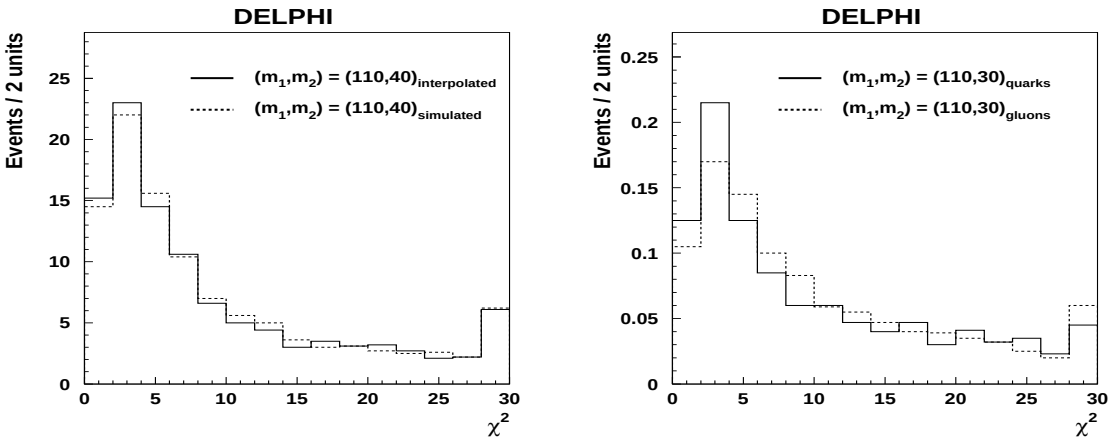

Figure 7: The lefthand plot shows with the solid line the distribution of the variable $\chi^2(m_1, m_2)$ for the compatibility with a (110,40) mass hypothesis when interpolating from the nearest simulated samples at (110,30) and (110,50) GeV/c^2. It is compared with the 'true' (dashed line) distribution from a simulated sample at (110,40). The righthand plot shows the same distribution for two different simulated samples: a Higgs boson decaying into either $q\bar{q}$ (solid line) or gg (dashed line) to indicate the worse mass resolution for a purely gluonic final state. In each distribution, overflows have been included in the last bin.

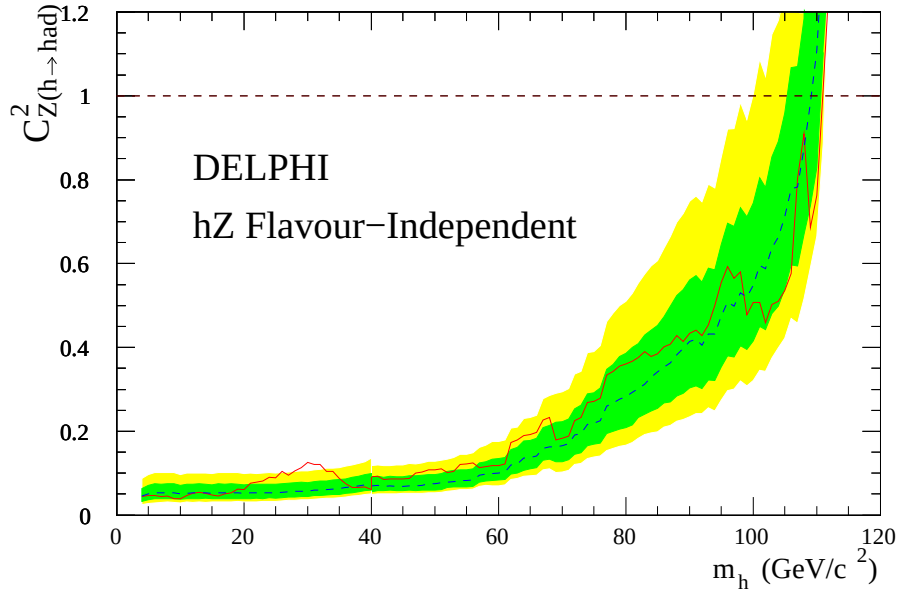

Figure 8: Excluded hZ cross-section at 95% confidence level relative to that of the SM Higgs boson as a function of the Higgs boson mass in case of direct decay of the Higgs boson into hadrons. The observed exclusion (solid line) is shown together with the median exclusion expected in the absence of signal (dashed line). The bands correspond to the 68.3% and 95% confidence intervals for the expected limit from background-only experiments.

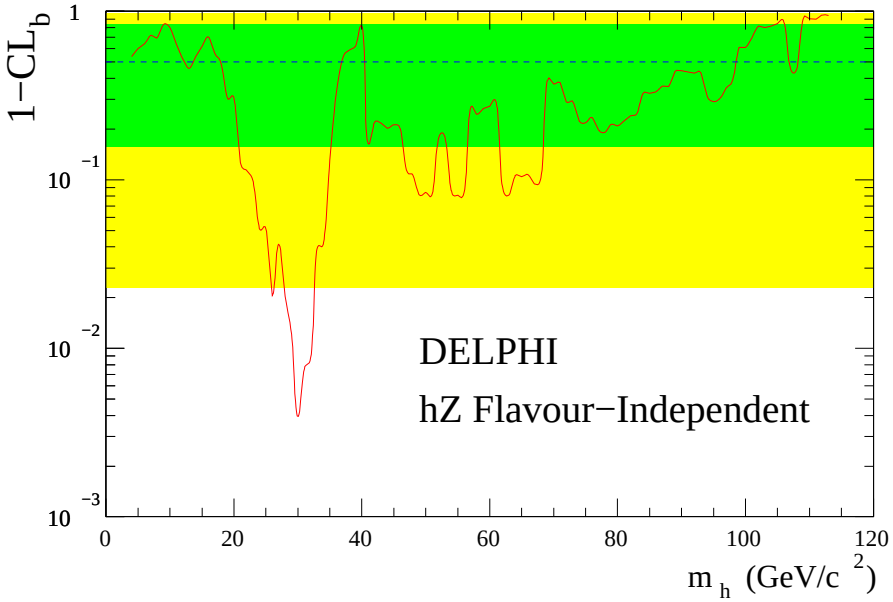

Figure 9: Confidence levels in the background hypothesis as a function of the Higgs boson mass, computed with the likelihood ratio technique [22]. Curves are the observed confidence (solid) and expected median (dashed) confidence from background-only experiments, while the bands correspond to 68.3% and 95% confidence intervals for the expected 1-CL_b from background-only experiments.

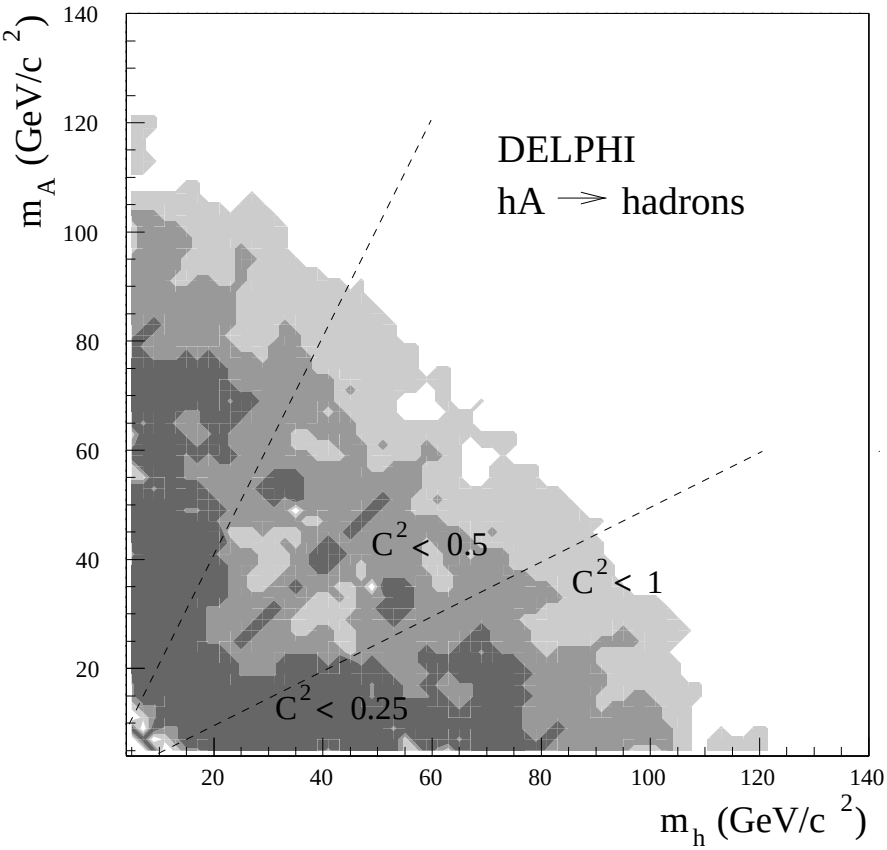

Figure 10: Excluded regions in the ($m_{\rm h}$,$m_{\rm A}$)-plane at 95% confidence level, for Higgs cross-sections and branching ratios into hadrons such that $C^2_{hA\to had}$ =1 (light grey), 0.50 (intermediate grey), and 0.25 (dark grey). The dashed lines indicate the border where intermediate decays of heavy into a pair of lighter Higgs bosons open kinematically.